Shock Tube Test Time Limitation Due to Turbulent-Wall Boundary Layer

HAROLD MIRELS*
Aerospace Corporation, El Segundo, Calif

Shock tube test time limitation due to the premature arrival of the contact surface is analytically investigated for wholly turbulent-wall boundary layers The results are compared with those for wholly laminar-wall boundary layers It is found that, for a given shock Mach number M_s, the maximum possible test time (in a long shock tube) varies as $d^{6/4}p_\infty^{1/4}$ and d^2p_∞ for the turbulent and laminar cases, respectively (d = tube diameter, p_∞ = initial pressure) For $3 \lesssim M_s \lesssim 8$ in air or argon, it is found that the turbulent-boundary-layer theory for maximum test time applies, roughly, for $dp_\infty \gtrsim 5$, whereas the laminar theory applies, roughly, for $dp_\infty \lesssim 0\,5$ A transitional-boundary-layer theory is required when $dp_\infty \approx 1$ (d is in inches; p_∞ is in centimeters of mercury) When $dp_\infty \approx 5$, turbulent theory for both air and argon indicates test times of about one-half to one-fourth the ideal value for $x_s/d = 45$ to 150, respectively (x_s = length of low-pressure section) Higher values of dp_∞ result in more test time When $dp_\infty \approx 0\,5$, laminar theory indicates about one-half ideal test time for $x_s/d \approx 100$ Lower dp_∞ reduces test time Working curves are presented for more accurate estimates of test time in specific cases Boundary-layer closure occurs, in long shock tubes, when $M_s \lesssim 1\,2$ and $M_s \lesssim 3$ for laminar and turbulent boundary layers, respectively

I Introduction

IN an ideal inviscid shock tube, the separation distance between shock and contact surface increases linearly with distance from the diaphragm (Fig 1) In a real shock tube, however, the wall boundary layer between the shock and contact surface acts as an aerodynamic sink and absorbs mass from this region This causes the contact surface to accelerate and the shock to decelerate and reduces the separation distance l below the ideal value The separation distance approaches a limiting (maximum) value l_m At this limiting condition, the shock and contact surface both move with the same velocity (Fig 1) The limiting separation distance is that at which the mass flow entering the shock equals the boundary-layer mass flow moving past the contact surface

Separation distance imposes an upper bound on the test time in shock tubes (Nonuniformity of the flow between shock and contact surface may further reduce test time The amount of flow nonuniformity which can be tolerated depends on the nature of the experiment and the instrumentation) It is thus important to know separation distance as a function of distance from the diaphragm in order to estimate test times in shock tubes

The effect of a laminar-wall boundary layer on separation distance has been studied experimentally by Duff[1] and both experimentally and analytically by Roshko[2] and Hooker [3] Some aspects of the analyses presented in Refs 2 and 3 are modified in Ref 4 These references can be used to estimate test time in low-pressure shock tubes (roughly, those shock tubes with initial pressures of the order of 1 mm Hg or less, currently being used to study dissociation, ionization, and other rate phenomena) The test time limitation in low-pressure shock tubes has received considerable attention because the upper limit on test time is proportional to d^2p_∞,[2] and very low d^2p_∞ can result in virtually no usable test time (d = tube diameter, p_∞ = initial pressure)

The effect of a turbulent-wall boundary layer on separation distance has been treated only by Anderson [5] It is interesting to note that Anderson was the first to blame less than ideal shock tube test time on the premature arrival of the contact surface Anderson showed, for two practical examples, that mass loss to a turbulent-wall boundary layer reduced the theoretical test time by about a half This was in agreement with a rule-of-thumb presented in Ref 6 for shock tubes used to study re-entry heat transfer In Ref 6, it was stated that 40 to 70% of theoretical test time was generally obtained, and 50% was proposed as a mean value (The test time referred to was the period of essentially uniform conditions The reduction from the ideal value was attributed, in Ref 6, to mixing at the interface and flow nonuniformity associated with shock attenuation rather than to the premature arrival of the contact surface) Since test time did not appear to represent a serious problem in re-entry heat-transfer shock tube studies, the work of Anderson did not find widespread application

As previously noted, the effect of a laminar boundary layer on shock tube test time is now receiving considerable attention [1-4] It is therefore felt that it is worthwhile to develop the turbulent-boundary-layer case beyond the preliminary work of Anderson Anderson presented a first estimate of the variation of separation distance with distance from the diaphragm for a particular initial pressure (10 cm Hg) and two tube diameters (1 5 and 4 in) In the present paper, the problem is formulated more accurately,† and the results are presented in nondimensional form so as to be applicable for arbitrary initial pressures and tube diameters Criteria are established to define when turbulent-wall boundary-layer theory is applicable and when laminar-wall boundary-layer theory is applicable The development here is parallel to that used in Ref 4 for the laminar case

The present solution is primarily intended for the case where the wall boundary layer introduces sizable reductions in test time When the wall boundary layer introduces only small perturbations of the ideal test time, the linearized methods of Refs 7 and 8 are more appropriate

II Maximum Separation Distance

When the maximum separation distance is reached, both shock and contact surface move with the same velocity The flow between the shock and contact surface may then be

Received June 24, 1963; revision received November 4, 1963

* Head, Advanced Propulsion and Fluid Mechanics Department, Aerodynamics and Propulsion Research Laboratory Associate Fellow Member AIAA

† In Anderson's solution, the separation distance first increases, reaches a maximum, and then decreases with distance from the diaphragm, as will be discussed later

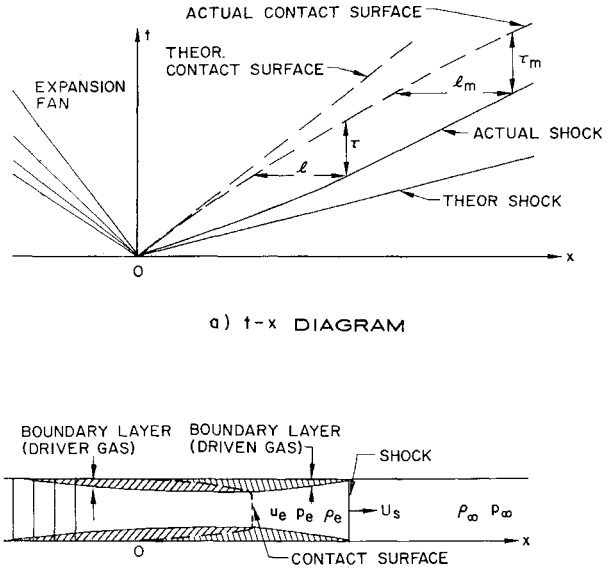

Fig 1 Boundary-layer effect on shock tube flow

viewed as steady in a coordinate system in which the shock is stationary In this shock-stationary coordinate system, the wall moves with velocity u_w (which equals the shock velocity U_s in the laboratory system) This steady flow is investigated in this section with the primary object of determining the maximum separation distance between the shock and the contact surface The variation of separation distance with distance from the diaphragm is treated in Sec III

The steady flow is illustrated in Fig 2a The shock is located at $l = 0$, and the freestream portion of the contact surface is located at $l = l_m$ The flow upstream of the shock is denoted by subscript ∞ and moves with velocity u_w, as does the wall Freestream conditions between the shock and the contact surface are denoted by subscript e Freestream conditions directly downstream of the shock have the additional subscript 0 The percentage of mass flow in the boundary layer increases with l such that all the mass flow is in the boundary layer at l_m, and the freestream is stationary at that location

The physical parameters upon which l_m depends can be found as follows The flow rate through the shock $\dot{m}$ is

$$\dot{m}_s = (\rho_e u_e)_0 A = \rho_\infty u_w A \tag{1a}$$

where A is the cross-sectional area of the tube If it is assumed that the boundary layer is thin relative to the tube radius, the mass flow in the boundary layer at the contact surface location $\dot{m}_c$ can be characterized by

$$\dot{m}_c = L\rho_{w\,0}(u_w - u_{e\,0})\delta_R \tag{1b}$$

where

$$\delta_R \equiv \beta l_m^{1-n}\left(\frac{\nu_{w,0}}{u_w - u_{e\,0}}\right)^n \tag{1c}$$

Here L is the perimeter of the tube; δ_R is a characteristic boundary-layer displacement thickness at l_m; $\rho_{w\,0}$ and $u_w - u_{\,0}$ are characteristic densities and velocities, respectively; β is a constant; and $n = \frac{1}{2}$ for laminar and $\frac{1}{5}$ for turbulent boundary layers Equating Eqs (1a) and (1b) yields

$$l_m^{1-n} = \frac{d}{4\beta}\frac{\rho_{,0}}{\rho_{w\,0}}\frac{u_{e,0}}{u_w - u_{\,0}}\left(\frac{u_w - u_{e,0}}{\nu_{w\,0}}\right)^n \tag{2}$$

where $d = 4A/L$ is the hydraulic diameter of the tube

Assume that the temperature upstream of the shock is at a standard condition so that $T_\infty = T_{\,t}$, $a_\infty = a_{\,t}$, and $\mu_\infty = \mu_{\,t}$ Also, assume that the wall remains at its initial temperature so that $T_w = T_{\,t}$ Equation (2) can now be put in the form

$$\left(\frac{p_{st}}{p_\infty}\right)^n \frac{l_m^{1-n}}{d} = \frac{1}{4\beta}\left(\frac{p_\infty}{p_{e\,0}}\frac{W}{W-1}\right)^{1-n} M^n \left(\frac{\rho a}{\mu}\right)_{st}^n \tag{3}$$

where $W = u_w/u_{\,0} = \rho_{\,0}/\rho_\infty$; $M = u_w/a_\infty$; and $p_{\,t}$ is a standard pressure, usually taken to be 1 atm For $n = \frac{1}{2}$, these equations reduce to those presented in Ref 4 For $n = \frac{1}{5}$, Eq (3) becomes

$$\left(\frac{p_{st}}{p_\infty}\right)^{1/4} \frac{l_m}{d^{5/4}} = \left(\frac{1}{4\beta}\right)^{5/4} \frac{p_\infty}{p_{e\,0}}\frac{W}{W-1} M^{1/4}\left(\frac{\rho a}{\mu}\right)_t^{1/4} \tag{4}$$

The right-hand side of Eq (3) depends primarily on M_s For a given M, $l_m \sim d^2 p_\infty$ for a laminar boundary layer, and $l_m \sim d^{5/4} p_\infty^{1/4}$ for a turbulent boundary layer Therefore, for turbulent boundary layers, l_m is less sensitive to variations of d and p_∞ than is the case for laminar boundary layers

Equation (4) does not yield numerical results for l_m unless an accurate estimate of β is available Actually, β must be found from l_m, rather than vice versa That is, Eq (2) is taken as defining β:

$$\beta \equiv \frac{d}{4 l_m^{1-n}}\frac{p_\infty}{p_{e\,0}}\frac{W}{W-1}\left(\frac{u_w - u_{\,,0}}{\nu_{w\,0}}\right)^n \tag{5}$$

and l_m is found as accurately as possible from a consideration of the boundary-layer development in Fig 2a A first estimate for β, termed β_0, is made below by assuming the boundary layer to develop in a uniform external stream An improved estimate, termed β_1, is then made by considering a variable external stream and employing the concept of local boundary-layer similaritv

A Uniform External Freestream Approximation

Boundary layer development for the case of an external freestream that does not vary with l is illustrated in Fig 2b and is discussed in Appendix A Let l_m correspond to the value of l at which the *excess mass flow* in the boundary layer equals the mass flow entering through the shock The mass flow past the contact surface is then

$$\frac{\dot{m}_c}{L(\rho\, u)_0} = -\delta_m^* \equiv K_0 l_m^{4/5}\left(\frac{\nu_{w,0}}{u_w - u_{e\,0}}\right)^{1/5} \tag{6}$$

where δ_m^* is the displacement thickness at l_m, and K_0 is a function defined in Appendix A Equating Eqs (1b, 1c, and 6) then yields

$$\beta_0 = \frac{p_\infty}{p_{\,0}}\frac{W}{W-1}K_0 \tag{7}$$

Values of β_0 have been computed for $\gamma = \frac{7}{5}$, $\sigma = 0\,72$ and $\gamma = \frac{5}{3}$, $\sigma = 0\,67$ using the turbulent-boundary-layer theory of Appendix A together with the Sutherland viscosity law (γ = ratio of specific heats, σ = Prandtl number) Values of β_0 have also been computed for the flow behind strong shocks in air at initial pressures of 0 5 and 10 cm Hg These four cases are further identified in Fig 3a The numerical results for β_0 are listed in Table 1 These values of β_0 can be used to find turbulent-boundary-layer displacement thickness [Eqs (6) and (7)] and will be used later to find β_1

It is expected that these values of β_0 will overestimate l_m, particularly for shock Mach numbers that are not large, because the relative velocity between the wall and the freestream increases from $u_w - u_{\,0}$ at $l = 0$ to u_w at l_m (compare Figs 2a and 2b) Hence, the excess mass flow in the boundary layer will be greater at a given l than the excess obtained from the forementioned model This will result in smaller l_m and larger β than obtained from Eq (7) However, for very strong shocks, where $u_{\,0}$ is small relative to u_w, Eq (7) should give accurate results

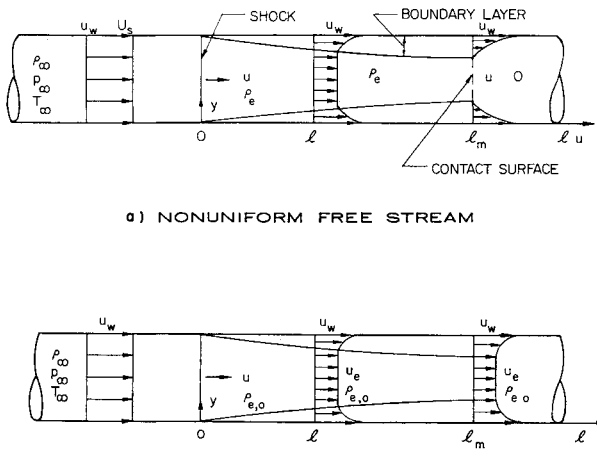

Fig 2 Flow between shock and contact surface in shock-stationary coordinate system

B Local Similarity Approximation

In this section, the streamwise variation of freestream properties due to the increase in boundary-layer mass flow with l is taken into account The development of the boundary layer and the variation in freestream properties are treated simultaneously The boundary-layer growth is found by assuming that at each station it is similar to a corresponding boundary layer developing in a uniform freestream behind a shock moving with uniform velocity (i e , local similarity)

Since the flow is steady (Fig 2a), the net mass flow through the shock equals the net mass flow at any station l Thus

$$A(\rho_e u)_0 = A\rho_e u_e + L\int_0^\infty (\rho u - \rho_e u_e)dy \tag{8}$$

In Eq (8), it is assumed that the boundary-layer thickness is small compared with d; thus the integrand is nonzero only in the region close to the wall Otherwise, for circular tubes, the coefficient L would have to be replaced by a factor $\pi(d - 2y)$ in the integrand of Eq (8) Define

$$\bar{\delta} \equiv \frac{4}{d}\frac{\rho_e u_e}{(\rho u)_0}(-\delta^*) \tag{9}$$

where δ^* is the boundary-layer displacement thickness based on the local freestream

$$\delta^* = \int_0^\infty \left(1 - \frac{\rho u}{\rho u}\right)dy \tag{10}$$

Note that $\bar{\delta}$ is the ratio of the excess mass flow through the boundary layer at l to the mass flow through the shock Thus $\bar{\delta}$ varies from 0 at $l = 0$ to 1 at $l = l_m$ Equations (8–10) then give

$$\bar{\delta} = 1 - \frac{\rho_e u_e}{(\rho_e u_e)_0} \tag{11}$$

which relates the freestream conditions to the local boundary-layer displacement thickness

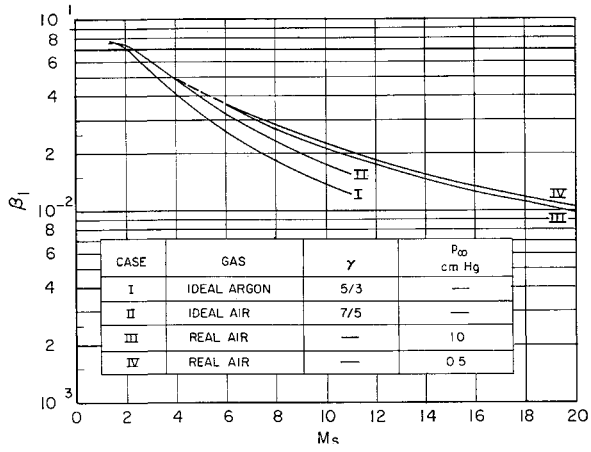

a) β_1 obtained from Eq (17) and Table 1

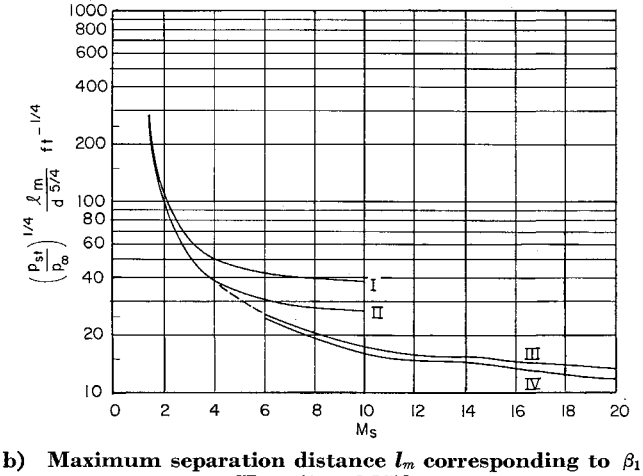

b) Maximum separation distance l_m corresponding to β_1 [Eqs (4 and 17)]

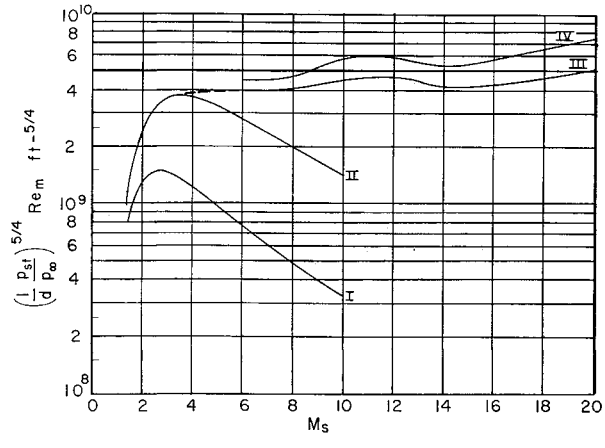

c) Reynolds number corresponding to l_m

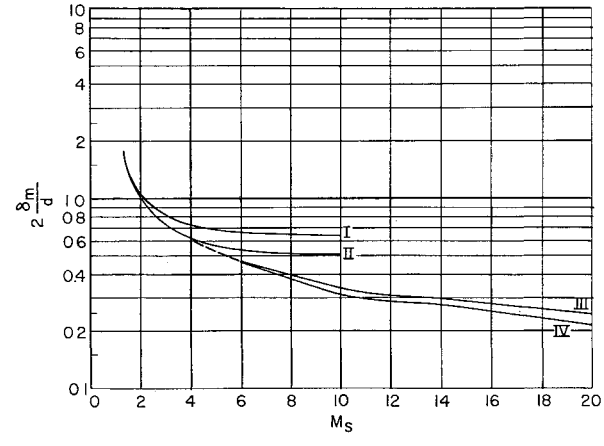

d) Boundary-layer thickness at l_m [Eq (18)]

Fig 3 Quantities defining maximum separation distance for turbulent-wall boundary layer, $T_t = T_w = 522° \times$ R, $p_{st} = 1$ atm For argon and air, respectively, $\sigma = 0\ 67, 0\ 72$; $r(0) = 0\ 875, 0\ 897$; Sutherland constant = 306°R, 198 6° × R; $(\delta^*/\delta)/(1 - W) = 0\ 176, 0\ 157$; B = $2\frac{7}{3}$; $(\rho\alpha/\mu)_{st} = 7\ 39 \times 10^6$ ft^{-1}, $6\ 93 \times 10^6$ ft^{-1}

The concept of local similarity is now introduced It is assumed that the boundary layer profile at each l corresponds to the profile for a boundary layer associated with a uniform freestream (equal to the local freestream) and a wall velocity u_w The origin of this fictitious boundary layer is at l_i, which is initially an unknown function of l The origin l_i is chosen such that the excess flow in the boundary layer at each l has the correct local value If M is sufficiently large that variations in ρ and p_e can be ignored, Eqs (11) and (A11a) become

$$\bar{\delta} = 1 - V \tag{12a}$$

$$\bar{\delta} = H_e(l - l_i)^{4/5} \tag{12b}$$

where $V = u/u_0$, and H_e is a function of the local freestream as defined in Eq (A11b) The problem is now to solve these equations simultaneously to find $\bar{\delta}$ as a function of l The value of l at $\bar{\delta} = 1$ defines l_m and thus provides an improved estimate for β

Assume that the local rate of growth of $\bar{\delta}$ follows the local similarity law $\bar{\delta} = H_e(l - l_i)^{1-n}$ (with H_e and l_i considered constant at the local values) This is the approach used in Ref 4 It follows that

$$\frac{\Delta\bar{\delta}}{\bar{\delta}} = (1 - n)\frac{\Delta l}{l - l_i} = (1 - n)\left(\frac{H_e}{\bar{\delta}}\right)^{1/(1-n)}\Delta l \tag{13}$$

For $n = \frac{1}{2}$, this expression is the same as that derived in Ref 4 For $n = \frac{1}{5}$, Eqs (13) and (12a) give, in integral form,

$$l = \frac{5}{4}\int_V^1 \frac{(1 - V)^{1/4}}{H_e^{5/4}}\,dV \tag{14}$$

Substituting Eq (A11b) for H_e and considering the limit $V = 0, l = l_m$ yields

$$\left(\frac{4K_0}{d}\right)^{5/4}\left(\frac{\nu_{w,0}}{u_w - u_0}\right)^{1/4} l_m = \frac{5}{4}\int_0^1 (1 - V)^{1/4} \times \frac{W + BV}{W + B}\left(\frac{W - 1}{W - V}\right)^2 dV \equiv F \tag{15}$$

The constant B is defined in Appendix A

Equation (15) has been numerically integrated for $B = \frac{7}{3}$ and 2, which correspond to air and argon, respectively The numerical results have been correlated to within 3% for $W \geq 1\,5$ and to within 2% for $W \geq 2\,0$ by the expression

$$F = W(W - 1)/(W^2 + 1\,25W - 0\,80) \tag{16}$$

Substitution of Eq (15) into Eq (5), to eliminate l_m, yields the following value for β_1:

$$\beta_1 = \frac{\beta_0}{F^{4/5}} = \beta_0\left[\frac{W^2 + 1\,25W - 0\,80}{W(W - 1)}\right]^{4/5} \tag{17}$$

This expression has been used with the values of β_0 in Table 1 to obtain corresponding values of β_1 These values are presented graphically in Fig 3a

C Numerical Results for l_m, Re_m, and $2\delta_m/d$

The values of β_1 in Fig 3a have been used to compute l_m from Eq (4) The results are given in Fig 3b Standard conditions were assumed to be $T_t = 522°\text{R}$ and $p_t = 76$ cm Hg, so that $(\rho a/\mu)_t = 6\,93 \times 10^6\ \text{ft}^{-1}$ for air and $(\rho a/\mu)_t = 7\,39 \times 10^6\ \text{ft}^{-1}$ for argon

In order for the present theory to be valid, it is necessary that the boundary layer be turbulent This will be the case if the Reynolds number at l_m is considerably larger than the transition Reynolds number An appropriate Reynolds number, based on l_m, is $Re_m = u_0(W - 1)^2 l_m/\nu_0$ The parameter $[p_t/(dp_\infty)]^{5/4}Re_m$ is plotted in Fig 3c The transition Reynolds number has been investigated[9] and is in the range $0\,5 \leq Re_t \times 10^{-6} \leq 4$ for $1 \leq M_s \leq 9$ It appears to increase markedly for larger M because of the stabilizing effect of the low wall temperatures, but only limited data are available The present turbulent-boundary-layer theory should be applicable if Re_m is significantly larger than Re_t (say, $Re_m \geq 5Re_t$)

It has also been assumed [e g , Eqs (1) and (8)] that the boundary layer thickness is small relative to the tube radius This condition will be satisfied if $2\delta_m/d$ is small Here, δ_m is the boundary layer thickness at l_m If δ_m is assumed to vary as in the case of a uniform external stream, it can be shown that

$$\frac{2\delta_m}{d} = \frac{1}{2}\frac{F^{4/5}}{W - 1}\left(\frac{1 - H}{\delta^*/\delta}\right) \tag{18}$$

This parameter is plotted in Fig 3d It is seen that $2\delta_m/d \geq 1$ for $M \leq 2$ so that the assumption of a small boundary-layer thickness is violated For argon considered as an ideal gas (case I), the quantity $2\delta_m/d$ does not go below 0 6; and for ideal air (case II), it does not go below 0 45 The real-gas solutions for air (cases III and IV) have values below 0 5 for $M \geq 6$ However, it should be noted that $2\delta_m/d$ provides a very conservative estimate for the validity of the present theory What is mainly required is that the boundary layer not become fully developed (i e , $2\delta_m/d < 1$) and that the integrand in Eq (8) not require the factor $\pi(d - 2y)$ (for circular cross sections) The second of these conditions is probably satisfied when $2\delta_m/d < 1$ since most of the boundary layer excess mass flow occurs in the portion of the boundary layer near the wall For example, by neglecting density effects and assuming a one seventh power velocity profile it can be shown that 56% of the excess mass flow occurs within a distance δ_m 4 from the wall The higher gas density at the wall (particularly for strong shocks) will considerably increase the fraction of excess mass flow in this distance The present approach is therefore considered valid for $M \gtrsim 3$

Table 1 Values of β_0 [Eq (7)]

Case I[a]		Case II		Case III		Case IV	
M_s	β_0	M_s	β_0	M_s	β_0	M_s	β_0
1 41	0 0263	1 35	0 0253	6	0 0270	6	0 0283
1 73	0 0326	1 58	0 0332	8	0 0210	8	0 0220
2 24	0 0345	1 89	0 0389	10	0 0175	10	0 0188
3 00	0 0312	2 24	0 0413	12	0 0149	12	0 0157
3 46	0 0284	2 65	0 0413	14	0 0122	14	0 0129
4 12	0 0245	3 16	0 0391	16	0 0106	16	0 0116
5 20	0 0195	3 87	0 0348	18	0 0095	18	0 0104
6 08	0 0164	5 00	0 0282	20	0 0084	20	0 0094
7 55	0 0126	5 70	0 0248				
8 77	0 0105	6 71	0 0208				
10 82	0 0080	8 37	0 0161				
		9 75	0 0133				

[a] Cases I–IV are identified in Fig 3a

In earlier studies of shock tubes,[10] it was felt that closure of the boundary layer (i e , $2\delta/d = 1$) might define an upper limit to test time Figure 3d indicates that the limiting separation distance is reached, before the boundary layer closes, for $M_s \gtrsim 3$ However, for $M \lesssim 3$ boundary-layer closure occurs first The corresponding curve in Ref 4 indicates that laminar-boundary-layer closure occurs for $M \lesssim 1\,2$ These estimates are approximate, since they represent extrapolations of "thin boundary-layer" solutions

III Variation of Separation Distance with Distance from Diaphragm

In Sec II, the limiting value of the separation distance between the shock and contact surface was found as a function of M This value defines the test time in shock tubes that are sufficiently long to permit the separation limit to be reached In order to estimate test times in shorter shock tubes, it is necessary to consider the rate at which separation distance increases with distance of the shock from the diaphragm This problem is now discussed, using the approach in Ref 4 It will be assumed that the shock moves with uniform velocity and that the flow between the shock and contact surface is steady in a shock-fixed coordinate system

A Separation Between Shock and Contact Surface

Consider flow in a coordinate system in which the shock is fixed and the wall moves with velocity u_w Assume that at $t = 0$ the contact surface coincides with the shock, and at some later time t the portion of contact surface, which is in the free-stream, is located at l (Fig 2a) and is moving with local velocity u_e The problem is to find l as a function of t (In the present section, l is considered to be a dependent variable defining the location of the contact surface relative to the shock as a function of time)

For steady flow, the mass flow through the shock equals the mass flow through a control surface at l This yields an equation identical to Eq (11) For the present purposes it can be assumed that the excess mass flow in the boundary layer varies as l^{1-n} Then, $\bar{\delta} = (l/l_m)^{1-n}$ Also, it will be assumed that $\rho/\rho_0 = 1$ (valid for strong shock) These assumptions have been shown to be accurate,[4] except near $W = 1$, where the present solution for l_m is invalid anyway Equation (11) then becomes

$$(l/l_m)^{1-n} = 1 - (u_e/u_{e0}) \tag{19}$$

Introduce the nondimensional variables

$$X \equiv \frac{u_{,0}t}{l_m} \equiv \frac{x_s}{Wl_m} \qquad T \equiv \frac{l}{l_m} \tag{20}$$

where $x = u_w t$ is the distance of the shock from the diaphragm in laboratory coordinates Noting that $dl/dt = u_e$, write Eq (19) in the form

$$T^{1-n} = 1 - (dT/dX) \tag{21}$$

Integration yields

$$-(X/2) = \ln(1 - T^n) + T^n \qquad \text{for } n = \tfrac{1}{2} \tag{22a}$$

$$= \frac{5}{8}\left(\ln\frac{1 - T^n}{1 + T^n} - 2\tan^{-1}T^n + 4T^n\right) \qquad \text{for } n = \tfrac{1}{5} \tag{22b}$$

Equation (22a) was first derived by Roshko ‡

The variation of T with X is plotted in Fig 4 for $n = \frac{1}{2}, \frac{1}{5}$ Note that $T = X$ corresponds to an ideal (no boundary layer) shock tube The departure of the curves in Fig 4 from $T = X$ represents the departure from ideal performance For $X \lesssim 0\,1$, the departure is small, and for $X \gtrsim 10$, the separation distance equals the limiting value

‡ Equation (22b) was derived by E F Brocher in an as yet unpublished study of test time for the case of small departures from the ideal flow

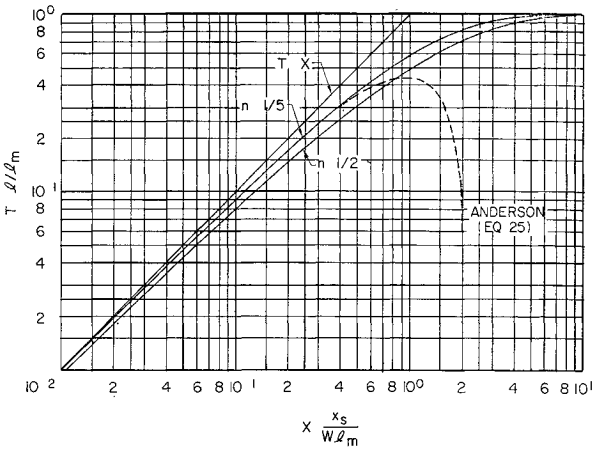

Fig 4 Separation distance as a function of distance from diaphragm [Eq (22)]

B Test Time

In the previous section, the separation distance was obtained as a function of t A quantity that is perhaps of greater interest is the test time (i e , the difference in time between the arrival of the shock and the arrival of the contact surface) at a fixed distance from the diaphragm, x_s This quantity will now be discussed

Designate the test time by τ For $x_s \to \infty$, $\tau \equiv \tau_m = l_m/u_w$ Define $\bar{\tau} \equiv \tau/\tau_m$, which is the test time at x divided by the test time at $x \to \infty$ If it is assumed that the shock moves with constant velocity, X and $\bar{\tau}$ are related[4] by $X = X_b -$

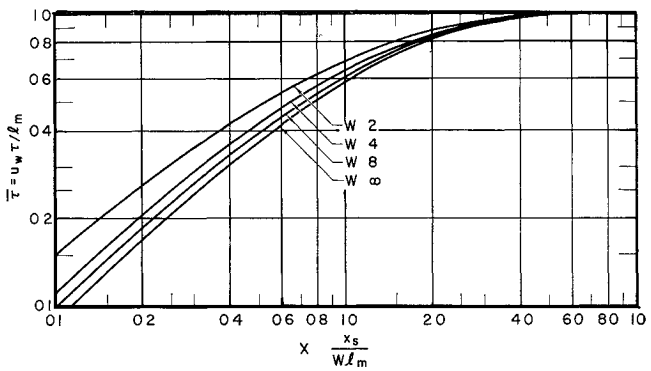

a) Normalized by maximum possible test time l_m/u_w

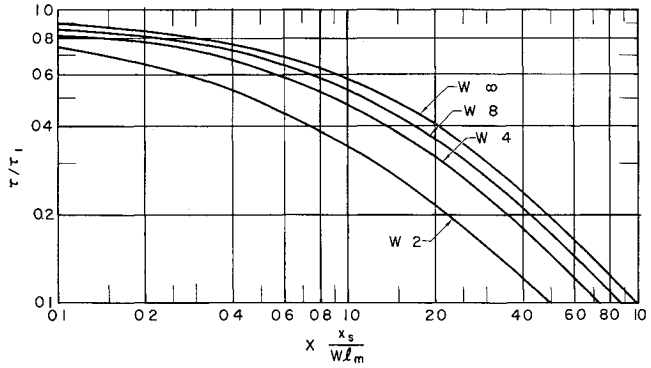

b) Normalized by ideal test time τ_i

Fig 5 Test time as a function of distance from diaphragm, $n = \frac{1}{5}$

(T_b/W) and $\bar{\tau} = T_b$, where X_b and T_b are corresponding values from Eqs (22) It then follows that, for $n = \frac{1}{5}$,

$$X = \frac{5}{4}\left[\ln\left(\frac{1 + \bar{\tau}^{0\,2}}{1 - \bar{\tau}^{0\,2}}\right) + 2\tan^{-1}\bar{\tau}^{0\,2} - 4\bar{\tau}^{0\,2}\right] - \frac{\bar{\tau}}{W} \quad (23)$$

The variation of $\bar{\tau}$ with X is plotted in Fig 5a for $W = 2, 4, 8, \infty$ For large W, $\bar{\tau} = T$

The parameter $\bar{\tau}$ compares the test time τ to the asymptotic test time l_m/u_w It is also of interest to compare τ to the test time for an ideal shock tube, $\tau_i = x/[(u_w - u_{e\,0})W]$ It can be shown that

$$\tau/\tau_i = [(W - 1)/W](\bar{\tau}/X) \quad (24)$$

Equations (23) and (24) can be solved to find τ/τ_i as a function of X and W The variation of τ/τ_i with X is plotted in Fig 5b for $W = 2, 4, 8, \infty$ For large W, $\tau/\tau_i = T/X$ The ratio $\tau/\tau_i = (W - 1)/WX$ for $X \gtrsim 5$ Note that, when $X = 1$, the test time is about one-half of the ideal value

Equations (22b) and (23) indicate that the relation between T and X is independent of W, whereas the relation between $\bar{\tau}$ and X does depend on W (due to the velocity of the contact surface relative to the shock) It may be desirable to attempt to correlate experimental $\bar{\tau}$, X data on the basis of T, X The data should then collapse to a single curve (Fig 4) If $\bar{\tau}_a$ is the measured test time at X_a, then the corresponding values of X and T are $X = X_a + \bar{\tau}_a/W$, $T = \bar{\tau}_a$ [4]

IV Comparison with Anderson's Solution

There is a basic difference between the separation distance solution presented by Anderson[5] and the one presented in this paper Anderson's method for finding the separation distance corresponding to a given shock location x is as follows He assumes that the shock moves with uniform velocity and finds the separation distance by equating $Al\rho_{\,0}$ to the difference between the ideal amount of shocked gas $Ax\,\rho_\infty$ and the amount of gas that has slipped past the contact surface However, Anderson's expression for the net mass loss past the contact surface is based on the *ideal* separation distance between shock and contact surface The latter he finds to be of the form $K_1 A\rho_\infty x_s^{9/5}$ (assuming a thin boundary layer), where K_1 is a function of M, d, p_∞, and is tabulated by Anderson The separation distance is then

$$l = (\rho_\infty/\rho_{e\,0})x\,(1 - K_1 x^{4/5})$$

If the nondimensional variables T, X are introduced, where l_m is based on the uniform freestream boundary layer approximation (i e , β_0), the latter equation becomes

$$T = X(1 - \tfrac{5}{9}X^{4/5}) \quad (25)$$

This is plotted in Fig 4 It is seen that, as X increases, T first increases, reaches a maximum of $T = \frac{4}{9}$ at $X = 1$, and then decreases For $X > (\frac{9}{5})^{5/4}$, T becomes negative Hence, Anderson's solution has a considerably different behavior than does the present solution, except for small X

If the freestream is assumed to remain uniform, the mass flow past the contact surface at any instant is proportional to $l^{4/5}$ The net mass loss since the start of the motion for a shock moving with uniform velocity is proportional to

$$\int_0^{x_s} l^{4/5}dx$$

For small x, where l varies linearly with x, the net mass loss has the form $x^{9/5}$, as derived by Anderson For large x, l approaches l_m, and the net mass loss tends to become proportional to $l_m^{4/5}x$, which is considerably smaller than the $x^{9/5}$ dependence used by Anderson Thus, Anderson's solution overestimates the mass loss and underestimates the test time for large x This accounts for the differences in the behavior of the two solutions

V Discussion

The present results can be used to estimate shock tube test time reduction due to mass loss to a turbulent-wall boundary layer The procedure is as follows First, Re_m is found from Fig 3c for given M_s, d, and p_∞ If this is substantially larger than Re_t (say $Re_m \geq 5\,Re_t$), the limiting separation between shock and contact surface will be due mainly to a turbulent boundary layer Hence the turbulent-boundary layer analysis can be used to estimate major reductions in shock tube test time Next, l_m is found from Fig 3b, and the value of $X = x/Wl_m$ can be determined for a given test section distance from the diaphragm Finally, the test time can be found from Fig 5

If Re_m, based on a laminar boundary layer, is less than Re_t, laminar-boundary layer theory is applicable, and a similar procedure is followed using the corresponding curves in Ref 4

For a given M_s, the value of Re_m depends primarily on dp_∞ Values of Re_m are plotted vs M for fixed values of dp_∞ in Figs 6a and 7a; the product dp_∞ has the units inches and centimeters of mercury Also plotted in these figures are estimated values of Re_t and 5 Re_t (It was assumed that Re_t varies linearly on the loglog plot from $Re_t = 0\,5 \times 10^6$ at $M_s = 1$ to $Re_t = 4 \times 10^6$ at $M = 9$ The curves are not continued beyond $M = 9$ because of uncertainty in Re_t) Turbulent-boundary-layer theory for finding l_m is applicable for values of dp_∞ which result in $Re_m \gtrsim 5\,Re_t$ These values (from Fig 6a) are as follows: for air, $dp_\infty \geq 4$ for $M_s = 3$ and $dp_\infty \geq 10$ for $M = 8$; for argon, $dp_\infty \geq 2$ for $M_s = 3$ and $dp_\infty \geq 10$ for $M = 8$ Similarly, laminar-boundary-layer theory is applicable when $Re_m \leq Re_t$, or (from Fig 7a) when the following holds true: for air, $dp_\infty \leq 0\,3$ for $M_s = 3$ and $dp_\infty \leq 0\,3$ for $M_s = 8$; for argon, $dp_\infty \leq 0\,6$ for $M_s = 3$ and $dp_\infty \leq 1$ for $M_s = 8$ It follows that, roughly, turbulent theory for maximum separation distance applies for $dp_\infty \gtrsim 5$ and laminar theory applies for $dp_\infty \lesssim 0\,5$, for $3 \leq M_s \leq 8$ A transitional-boundary-layer theory is required to find the maximum separation when $dp_\infty \approx 1$

In Figs 6b and 7b, x_s/Xd is plotted vs M for various dp_∞ The ordinate may be viewed as the value of x/d corresponding to $X = 1$, that is, the length-to-diameter ratio that results in about one-half the ideal test time For air or argon turbulent boundary layers and $M_s > 3$, $x_s/Xd \approx 45, 80, 140$ for $dp_\infty \approx 5, 50, 500$ (Thus, a shock tube with $dp_\infty \approx 5$ and $x/d \approx 50$ will have about half the ideal test time) Similarly, for air or argon laminar boundary layers, Fig 7b shows $x/Xd \approx 100, 10$, and 1 for $dp_\infty \approx 0\,5, 0\,05$, and $0\,005$, respectively

Before the present generation of low-pressure shock tubes,§ the typical low-pressure section of a shock tube had an internal diameter in the range 1 in $\leq d \leq 4$ in and a length-to-diameter ratio in the range 40–150 [10] Longer tubes were sometimes used, particularly in studies of shock attenuation; for example, a 2-in $\times$ 40-ft tube ($x_s/d = 240$) was used in Ref 11, and a 3 75-in $\times$ 120-ft tube ($x_s/d = 384$) in Ref 12

In a given shock tube, the largest reduction in test time, due to a wholly turbulent boundary layer, occurs at $dp_\infty \approx 5$ in -cm-Hg, for which $x_s/Xd \approx 45$ Tubes with $x_s/d \approx 45$ will have $X = 1$, or around half the theoretical test time (see Fig 5b) Tubes with $x/d \approx 150$ will have $X \approx 3$, or around one-fourth of the ideal test time (The 40% lower limit on test time, noted in Ref 6 and discussed in Sec I, is therefore not sufficiently low for this case) With regard to the larger values of x_s/d considered in Refs 11 and 12, it might be noted that $X \approx 5\,5$ for $x_s/d = 240$ and $X \approx 8\,5$ for $x_s/d = 384$ Here, the test times are approximately 0 15 and 0 1 of the ideal values, respectively For these values of X, the separation distance has reached its maximum value (Fig 4)

§ Present-day low-pressure tubes have low-pressure sections: 6 in $\times$ 30 ft (Avco), 24 in $\times$ 50 ft (Avco), 17 in $\times$ 36 ft (Aerospace), 17 in $\times$ 70 ft (Caltech)

The smallest reduction in test time, due to a wholly laminar boundary layer, occurs when $dp_\infty \approx 0\,5$ From the results given in Ref 4, it can be seen that the test time is about one-half the ideal value when $x_s/d \approx 100$ The test time is slightly larger than the corresponding value for a turbulent boundary layer with $dp_\infty \approx 5$

It is thus seen that, for a given shock tube, operation at an initial pressure such that $dp_\infty \approx 5$ results in a *local* minimum in the maximum possible test time Higher values of dp_∞ will result in thinner turbulent boundary layers and, therefore, more test time With a decrease in dp_∞, the onset of a wholly laminar boundary will first tend to increase the test time; however, with further decrease in dp_∞, the boundary-layer mass flow will increase, and severe test time limitations will occur

VI Concluding Remarks

The effect of wholly laminar- and wholly turbulent wall boundary layers on shock tube test time has been discussed

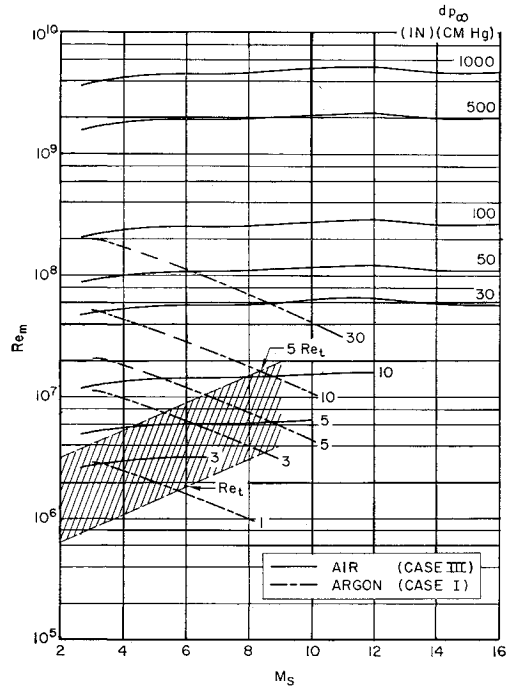

a) Re_m

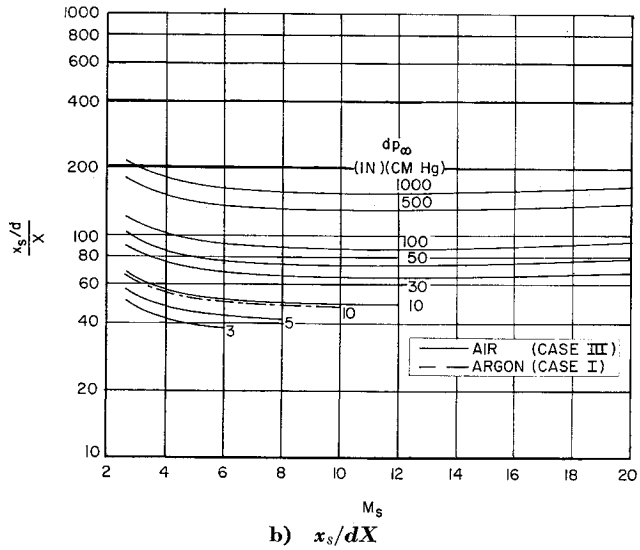

b) x_s/dX

Fig 6 Dependence of Re_m and x_s/dX on M_s and dp_∞ for turbulent boundary layer

It has been shown that, for a given shock Mach number, the maximum test time τ_m and separation distance l_m depend primarily on d^2p_∞ for $n = \frac{1}{2}$ and on $d^{5/4}p_\infty^{1/4}$ for $n = \frac{1}{5}$ Hence the laminar wall boundary-layer case is more sensitive to d and p_∞ Boundary layer closure occurs, in long shock tubes, when $M \lesssim 1\,2$ and $M \lesssim 3$ for laminar and turbulent boundary layers, respectively

Examples of previous studies have been noted where turbulent-wall boundary layers have reduced the test time from 0 1 to 0 5 of the ideal value The rule-of-thumb (see Sec I) that assumes about one-half of the ideal test time to be actually

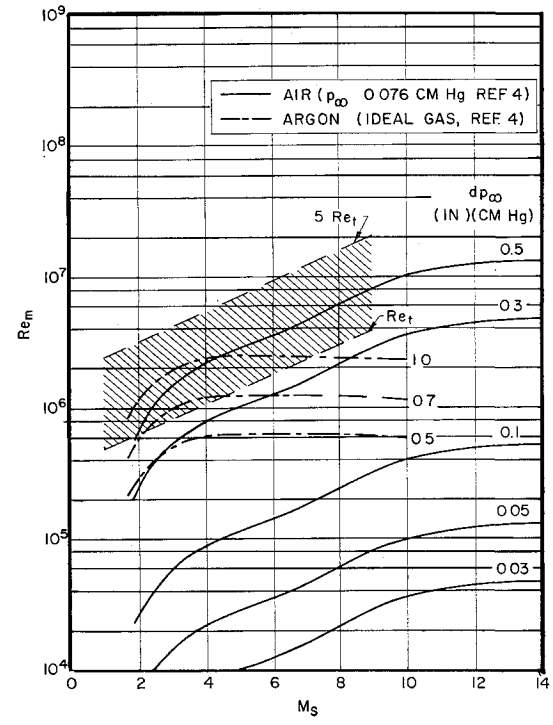

a) Re_m

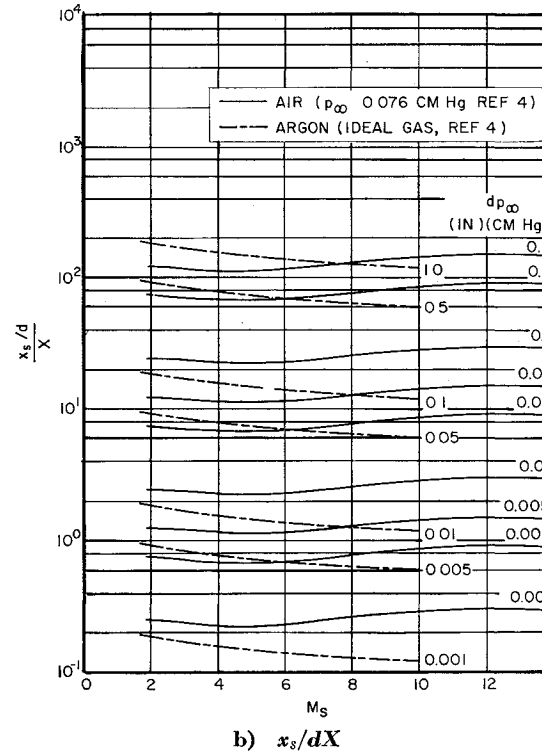

b) x_s/dX

Fig 7 Dependence of Re_m and x_s/dX on M_s and dp_∞ for laminar boundary layer

available is therefore not dependable The methods outlined herein should be used to estimate test time when necessary

It should be kept in mind that the present calculations actually provide an upper limit on the test time It is also necessary to consider 1) nonideal diaphragm rupture (which promotes interface mixing and causes nonideal flow near the diaphragm), and 2) flow nonuniformity between the shock and contact surface The degree of flow nonuniformity which can be tolerated in a shock tube depends on the nature of the aerodynamic test and the sensitivity of the instrumentation In some cases, it is desirable to incorporate a knowledge of the flow nonuniformity into the data reduction When the maximum separation is reached, the freestream flow nonuniformity can be estimated from

$$\rho_e u/(\rho u)_0 = 1 - (l/l_m)^{1-n} \tag{26}$$

by noting that, in shock-fixed coordinates, the flow is both steady and isentropic The flow corresponds to one-dimensional subsonic flow in an expanding channel with an effective area ratio $A/A_0 = (\rho u)_0/\rho u_e$ Equation (26) follows from Eq (11), with δ approximated by $(l/l_m)^{1-n}$

It should also be noted that the validity of the turbulent-boundary-layer theory used in the present report has not been fully established, particularly for strong shocks (see Appendix A) The present results are therefore intended as a first estimate for the effect of turbulent boundary layers on shock test time Experimental confirmation of these results would be desirable

Appendix A: Turbulent Boundary Layer behind Moving Shock

The turbulent boundary layer behind a moving shock was analytically studied in Refs 13 and 14 The general validity of some of the analytical results given in Refs 13 and 14 was experimentally established in Refs 15 and 9 for Mach numbers up to about 3 and 6, respectively Higher Mach numbers were not studied therein; hence the accuracy of the results in Refs 13 and 14 has not been fully established, particularly for strong shocks ($M_s > 6$) Nevertheless, the results in Refs 13 and 14 for displacement thickness will be summarized here and put in a form suitable for studying test time in shock tubes This will provide at least a first estimate of the effect of turbulent-wall boundary layers on shock tube test time

Assume that a shock moves with constant velocity, that the inviscid flow behind the shock is uniform, and that the wall boundary layer is turbulent (Fig 2b) The variation of displacement thickness with distance behind the shock (from Refs 13 and 14) is

$$-\delta^* \equiv \int_0^\infty \left[\frac{\rho u}{(\rho u)_0} - 1\right] dy \equiv K_0 l^{4/5} \left(\frac{\nu_{w,0}}{u_w - u_0}\right)^{1/5} \tag{A1}$$

where

$$K_0 \equiv 0\,0575 \frac{\delta^*/\delta}{1-W} \left(\frac{1-W}{\theta/\delta}\right)^{4/5} (W-1)^{9/5} \times \left[\frac{\mu_m}{\mu_w}\frac{\rho_w}{\rho_0}\left(\frac{\rho_m}{\rho_{e0}}\right)^3\right]^{1/5} \tag{A2}$$

where δ is the boundary-layer thickness and θ the momentum thickness The subscript m refers to conditions evaluated at a mean reference static enthalpy defined by

$$\frac{h_m}{h_0} = 0\,5\left(\frac{h_w}{h_0} + 1\right) + 0\,22\left(\frac{h_r}{h_{e0}} - 1\right) \tag{A3}$$

where h is the recovery enthalpy

In order to find K_0, it is necessary to evaluate

$$\frac{\delta^*/\delta}{1-W} = \frac{1}{W-1}\left\{7\frac{h_{e,0}}{h_w}\int_0^1 \frac{\zeta^6[W-(W-1)\zeta]}{1+b\zeta-c\zeta^2}d\zeta - 1\right\} \tag{A4a}$$

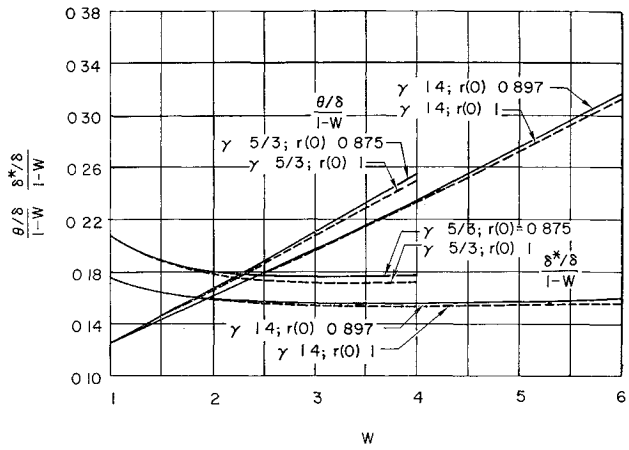

Fig 8 Turbulent-boundary-layer displacement and momentum thicknesses, ideal gas

$$\frac{\theta/\delta}{1-W} = 7\frac{h_{,0}}{h_w}\int_0^1 \frac{\zeta^6[W-(2W-1)\zeta+(W-1)\zeta^2]}{1+b\zeta-c\zeta^2}d\zeta \tag{A4b}$$

where

$$b = \frac{h_r}{h_w} - 1 \qquad c = \frac{h_r}{h_w} - \frac{h_{e,0}}{h_w} \tag{A5}$$

Equations (A4) can be evaluated for given b, c, and W, using the tables presented in Refs 13 and 14 For strong shocks, these tables require taking the differences of large, nearly equal numbers; thus the accuracy is reduced [Approximate expressions for evaluating Eqs (A4) for strong shocks are given in Appendix B] If convenient, it is preferable to evaluate δ^*/δ and θ/δ by the numerical integration of Eqs (A4)

Ideal Gas

Consider ideal gases with constant specific heat ratios γ obeying the perfect gas laws, $p = \rho RT$ and $h = c_p T$ For these gases,

$$\frac{h_r}{h_{e0}} = 1 + \frac{(W-1)^2}{ZW-1}r(0) \qquad \frac{h_w}{h_0} = \frac{W(Z-W)}{ZW-1} \tag{A6}$$

where $Z = (\gamma+1)/(\gamma-1)$, and $r(0) = (\sigma)^{1/3}$ is the recovery factor (σ = Prandtl number) Equations (A4) have been integrated, using Eqs (A6), for $\gamma = \frac{7}{5}$, $r(0) = 0\,897$ and for $\gamma = \frac{5}{3}$, $r(0) = 0\,875$ These values correspond to ideal air and to ideal argon, respectively The cases $\gamma = \frac{7}{5}$, $r(0) = 1$ and $\gamma = \frac{5}{3}$, $r(0) = 1$ have also been included to find the effect of $r(0)$ The results are given in Fig 8 and can be approximated by the following expressions:

$$\frac{\theta/\delta}{1-W} \equiv \frac{W+B}{C} = \frac{W+\frac{7}{3}}{\frac{8\,0}{3}} \qquad \text{for } \gamma = \tfrac{7}{5} \tag{A7a}$$

$$= \frac{W+2}{24} \qquad \text{for } \gamma = \tfrac{5}{3} \tag{A7b}$$

$$\frac{\delta^*/\delta}{1-W} \equiv D = 0\,157 \qquad \text{for } \gamma = \tfrac{7}{5},\ W \geq 2 \tag{A7c}$$

$$= 0\,176 \qquad \text{for } \gamma = \tfrac{5}{3},\ W \geq 2 \tag{A7d}$$

These expressions agree with the numerical integrations to within 3%

Equations (A7) have been used to evaluate K_0 as a function of M, using the Sutherland viscosity relation for argon and for air The results are given as cases I and II in Table 1 in terms of β_0

Table 2 Constants defining θ/δ and δ^*/δ for strong shocks [Eqs (B3)]

c/b	B	C	D	E
0 35	3 16	28 2	0 148	0 413
0 40	3 19	29 2	0 144	0 511
0 45	3 23	30 3	0 140	0 632
0 50	3 27	31 6	0 135	0 781

Real Gas

For strong shocks, Eqs (A6) are no longer valid The following procedure has therefore been used to obtain an estimate of the turbulent boundary layer behind a strong shock in air ($M_s \geq 6$)

The problem is to evaluate K_0 [Eq (A2)] for a strong shock First it was assumed that Eqs (A7a) and (A7c) could be used with W obtained from the equilibrium shock solutions of Ref 16 [Equations (A7a) and (A7c) agree with the limiting values of θ/δ and δ^*/δ obtained by strong shock assumptions, Eqs (B3), to within 5 and 8% for $W = 10$ and 15, respectively] It then only remains to evaluate the term [ ]$^{1/5}$ in Eq (A2) The energy equation for a strong shock gives

$$\frac{h_r}{h_{e\,0}} = 1 + \frac{W-1}{W+1}\, r(0) \tag{A8}$$

with $r(0) = 0\,897$ for air Reference 16 was used to find W and $T_{e\,0}/T_\infty = T_{\,0}/T_w$ for given M, p_∞, and $T_w = 300°\mathrm{K}$ It was then assumed that $\rho_{\,0}/\rho \approx h_w/h_{e,0} \approx T_w/T_{\,0}$ The latter, with Eq (A8), permits $h_m/h_{\,0} \approx T_m/T_{\,0} \approx \rho_{\,0}/\rho_m$ to be found and Eq (A2) to be evaluated The assumption that $h \approx T \approx 1/\rho$ is only approximately correct but should be sufficiently accurate for the present purposes {i e , evaluation of [ ]$^{1/5}$ in Eq (A2)}

The resulting values of K_0 are also given in Table 1 (in terms of β_0) This table, together with Eq (7), defines the turbulent boundary layer behind a strong shock in air It should be kept in mind that the turbulent-boundary layer theory of Refs 13 and 14 has not been verified for strong shocks and that further simplifying assumptions were made to obtain K_0

Boundary-Layer Theory for Local Similarity Approximation

The turbulent-boundary-layer equations will be put in a form that is appropriate for an origin at l_i, a wall velocity u_w, and freestream conditions u_e, ρ_e, which are isentropically related to conditions directly behind the shock ($u_{\,0}$, $\rho_{\,0}$) Equation (A1) becomes

$$-\delta^* = K\left(\frac{\nu_w}{u_w - u}\right)^{1/5}(l - l_i)^{4/5}$$

$$= K_0\left[\frac{K}{K_0}\left(\frac{\nu_w}{\nu_{u\,0}}\frac{W-1}{W-V}\right)^{1/5}\right]\left(\frac{\nu_{w,0}}{u_w - u_{e\,0}}\right)^{1/5}(l - l_i)^{4/5} \tag{A9}$$

where $V = u_e/u_{\,0}$ Equations (A7) have the form

$$\frac{\theta/\delta}{1 - (W/V)} = \frac{B + (W/V)}{C} \tag{A10a}$$

$$\frac{\delta^*/\delta}{1 - (W/V)} = D \tag{A10b}$$

where B, C, and D are constants If the freestream Mach number relative to the shock, $M_{\,0} = (u/a)_0$, is small (i e , strong shock), then the variation of fluid state properties in the freestream can be neglected ($\rho = \rho_{\,0}$; $p_e = p_{e\,0}$), and Eqs (A9) and (A10) then yield

$$\bar{\delta} = [4V(-\delta^*)/d] = H(l - l_i)^{4/5} \tag{A11a}$$

where

$$H_e = \frac{4K_0}{d}\left(\frac{W-V}{W-1}\right)^{8/5}\left(\frac{W+B}{W+BV}\right)^{4/5}\left(\frac{\nu_{w,0}}{u_w - u_{e\,0}}\right)^{1/5} \tag{A11b}$$

Note that $B = \frac{7}{8}$ for air and 2 for argon [Eq (A7)]

Appendix B: Limiting Forms for θ/δ and δ^*/δ

For the case of a weak shock, Eqs (A4) become

$$\frac{\delta^*/\delta}{1 - W} = \frac{\gamma}{8}[1 + 0(W-1)] \tag{B1a}$$

$$\frac{\theta/\delta}{1 - W} = \frac{1}{8}[1 + 0(W-1)] \tag{B1b}$$

For strong shocks, $b \gg 1$, $c \gg 1$, and the ratio c/b has a limiting value given by

$$\frac{c}{b} = \frac{r(0)}{\gamma + r(0)} \qquad \text{ideal gas} \tag{B2a}$$

$$= \frac{r(0)}{[(W+1)/(W-1)] + r(0)} \qquad \text{real gas} \tag{B2b}$$

If terms of order b^{-1} compared with 1 are neglected, Eqs (A4) yield

$$\frac{\delta^*/\delta}{1 - W} = \frac{1}{W-1}\left\{7\left(1 - \frac{c}{b}\right)\sum_{N=0}^{\infty}\frac{(c/b)^N}{7+N} \times \left[\frac{W}{6+N} + 1\right][1 + 0(b^{-1})] - 1\right\} \equiv D\left(\frac{W-E}{W-1}\right)[1 + 0(b^{-1})] \tag{B3a}$$

$$\frac{\theta/\delta}{1 - W} = 7\left(1 - \frac{c}{b}\right)\sum_{N=0}^{\infty}\frac{(c/b)^N}{(7+N)(8+N)} \times \left(\frac{2W}{6+N} + 1\right)[1 + 0(b^{-1})] \equiv \frac{W+B}{C}[1 + 0(b^{-1})] \tag{B3b}$$

The constants B, C, D, E have been evaluated for several values of c/b and are given in Table 2

For strong shocks in air, Eqs (A7a) and (A7c) agree with Eqs (B3) to within 5% for $W = 10$ and to within 8% for $W = 15$ Hence Eqs (A7a) and (A7c) are sufficiently accurate for a first estimate of θ and δ^* behind strong shocks in air

References

[1] Duff, R E , "Shock-tube performance at low initial pressure," Phys Fluids **2**, 207–216 (1959)

[2] Roshko, A , "On flow duration in low-pressure shock tubes," Phys Fluids **3**, 835–842 (1960)

[3] Hooker, W J , "Testing time and contact-zone phenomena in shock tube flows," Phys Fluids **4**, 1451–1463 (1961)

[4] Mirels, H , "Test time in low pressure shock tubes," Phys Fluids **6**, 1201–1214 (1963)

[5] Anderson, G F , "Shock-tube testing time," J Aerospace Sci **26**, 184–185 (1959)

[6] Rose, P H and Stark, W I , "Stagnation point heat-transfer measurements in dissociated air," J Aeronaut Sci **25**, 86–97 (1958)

[7] Mirels, H , "Attenuation in a shock tube due to unsteady-boundary layer action," NACA Rept 1333, supersedes NACA TN 3278 (1957)

[8] Mirels, H and Braun, W H , "Nonuniformities in shock tube flow due to unsteady boundary layer action," NACA TN 4021 (1957)

[9] Hartunian, R A , Russo, A L , and Marrone, P V , "Boundary-layer transition and heat transfer in shock tubes," J Aerospace Sci **27**, 587–594 (1960)

[10] Hall, J G, "Shock tubes Part II: Production of strong shock waves; shock tube applications, design, and instrumentation," Univ Toronto, Inst Aerophys Rev 12 (May 1958)
[11] Wittliff, C E and Wilson, M R, "Shock tube driver techniques and attenuation measurements," Cornell Aeronaut Lab Rept AD-1052-A-4 (August 1957)
[12] Jones, J J, "Experimental investigation of attenuation of strong shock waves in a shock tube with hydrogen and helium as driver gases," NACA TN 4072 (July 1957)
[13] Mirels, H, "Boundary layer behind shock or thin expansion waves moving into stationary fluid," NACA TN 3712 (1956)
[14] Mirels, H, "The wall boundary layer behind a moving shock wave," *Boundary Layer Research, Proceedings of the International Union of Theoretical and Applied Mechanics*, edited by H Gortler (Springer Verlag, Berlin, 1958), pp 283–293
[15] Martin, W A, "An experimental study of the turbulent boundary layer behind the initial shock wave in a shock tube," J Aerospace Sci 25, 644–652 (1958)
[16] Feldman, S, "Hypersonic gas dynamic charts for equilibrium air" Avco Res Rept 40 (1957)

JANUARY 1964 AIAA JOURNAL VOL 2, NO 1

Bearing Capacity of Simulated Lunar Surfaces in Vacuum

E C Bernett,* Ronald F Scott,† L D Jaffe,‡ E P Frink,§ and H E Martens¶
California Institute of Technology, Pasadena, Calif

The static bearing capacity of a granular material consisting of dry, crushed olivine basalt was determined in air and in a 10^{-6}-mm-Hg vacuum by means of cylindrical probes with a range of diameters Samples with various particle-size distributions (all below 35 mesh) were used for these tests It was found that the packing density of these granular materials was the factor that had the greatest effect on the bearing capacity The minimum bearing capacity of a loosely packed sample with a density of 1 25 g/cm³ was about 0 1 kg/cm² The maximum bearing capacity of a densely packed sample with density of 2 1 g/cm³ was about 7 kg/cm² The effects of vacuum were insignificant compared with the effect of packing density Direct shear tests indicated the cohesion in a few densely packed samples to be 1–2 × 10^4 dyne/cm² For the small probes used, the cohesion was estimated to contribute 85 to 95% of the observed bearing capacity for the densely packed samples but much less for the loosely packed samples

Introduction

THERE is a great deal of design work in progress on the equipment and instrumentation required for the lunar exploration program Precise information with regard to the nature and properties of the lunar surface would be very helpful to those involved in this work Past studies by optical and radio astronomy have indicated that large portions of the moon's surface are composed of a low-density material, probably in powder or porous form [1] It is therefore desirable to determine if properties of granular or porous materials are markedly different in high vacuum from those in air Studies have been carried out on powdered minerals in vacuum; the properties evaluated include resistance to dynamic penetration,[2,3] thermal conductivity,[4] and land locomotion values [5] In the present work, the static bearing capacity of rock powder was evaluated in air and high vacuum

Materials and Sample Preparation

The simulated lunar surface materials used in this bearing capacity study were prepared from unweathered olivine basalt collected from Pisgah Crater, San Bernardino County, Calif A detailed mineralogical description of this volcanic rock is given in Ref 2 The rough breakdown, crushing, pulverizing, and sizing operations were carried out as shown in the flow diagram (Fig 1) Six lots of granular material were obtained; two were well-graded, with nominal mesh sizes of −35 and −150; four were more uniformly sized, with nominal mesh sizes of −35 + 48, −48 + 65, −65 + 100, −100 + 150 A particle-size distribution analysis was carried out on each lot; the results are shown in Table 1 and Fig 2

The rock powders were stored in covered containers and were dry except for pickup of moisture from the air Checks made during the program by drying selected samples showed that the water content was always less than 0 1% by weight The density of the solid particles was found to average 2 97 g/cm³

It was desired to measure the bearing capacity of each lot of powder over a wide range of packing density Data at the lowest densities were of particular interest To obtain minimum packing densities, extreme care was taken during the loading of the powders into the sample holder A small scoop was used for this purpose, and each scoopful was gently placed on the surface of the material previously added Samples with packing densities as low as 1 25 g/cm³ were thus obtained The high-density samples were prepared by filling the container with powder and then tapping it on a solid surface With care in the tapping procedure, spalling of the surface could be avoided, and packing densities as high as 2 29 g/cm³ were obtained

Test Equipment and Procedure

The apparatus used for the bearing capacity measurements was a simple penetrometer (Fig 3) using interchangeable

Received July 2, 1963; revision received September 30, 1963 The work described herein represents one phase of research carried out at the Jet Propulsion Laboratory, California Institute of Technology, under Contract No NAS 7-100, sponsored by NASA

* Research Group Supervisor, Materials Research Section
† Associate Professor of Civil Engineering
‡ Chief, Materials Research Section Member AIAA
§ Research Engineer, Materials Research Section
¶ Assistant Chief, Materials Research Section